

Spin echo in spinor dipolar Bose–Einstein condensates

Masashi Yasunaga and Makoto Tsubota

Department of Physics, Osaka City University, Sumiyoshi-ku, Osaka 558-8585, Japan

(Dated: June 21, 2024)

We theoretically propose and numerically realize spin echo in a spinor Bose–Einstein condensate (BEC). We investigate the influence on the spin echo of phase separation of the condensate. The equation of motion of the spin density exhibits two relaxation times. We use two methods to separate the relaxation times and hence demonstrate a technique to reveal magnetic dipole–dipole interactions in spinor BECs.

PACS numbers: 03.75.Mn, 03.75.Nt

The discovery of spin echo in 1950 by Hahn was momentous in the field of magnetic resonance [1]. Hahn observed the recovery of a free induction decay signal of spins by using the combination of two $\pi/2$ pulses, naming the phenomenon “spin echo”. Carr and Purcell later proposed other methods of producing spin echo. The first, called “Method A”, uses the $\pi/2$ – π pulse sequence, while in “Method B” the echoes are obtained by applying many π pulses after a $\pi/2$ pulse [2]. Spin echo has contributed to the development of magnetic resonance, especially as a method of measuring the relaxation time for magnetic resonance imaging (MRI). MRI is used to visualize the structure of human bodies for medical examinations in hospitals. Spin echo is thus a field of physics with practical applications.

In low temperature physics, particularly for superfluid ^3He , NMR has made significant contributions in determining superfluid phases and revealing vortices and textures [3]. However, to date spin echo has not been studied in magnetic materials or superfluid ^3He . A natural development is applying spin echo to a spinor Bose–Einstein condensate (BEC). For this, it is important to consider the spin–spin relaxation mechanism. Recently, BECs with a magnetic dipole–dipole interaction (MDDI) have received considerable attention [4, 5, 6, 7, 8]. The MDDI may be closely related to the relaxation mechanism of the spins. ^{52}Cr BECs have been realized by Griesmaier *et al.* [9]. A ^{52}Cr atom has a magnetic moment six times larger than that of an alkali atom. Hence, a ^{52}Cr condensate clearly shows the effects of the MDDI as an anisotropic free expansion which depends on the orientation of the atomic dipole moments [10]. The magnitude of the MDDI can be controlled by modulating the s-wave scattering length [11]. Although the MDDI of alkali atomic BECs is quite small, it would be possible to observe the MDDI in the systems as well as in a ^{52}Cr BEC [12].

In this letter, we propose spin echo in a spinor BEC. Investigating spin echo will provide information on the MDDI, which is exhibited even by ^{87}Rb BECs.

First, we briefly review the general Bloch equation for spin relaxation and then review spin echo. A spin \mathbf{S} with gyro-magnetic ratio γ precesses with Larmor frequency

$\omega_L = \gamma H$ under a magnetic field $\mathbf{H} = H\hat{z}$ described by the equation of motion of the spin $d\mathbf{S}/dt = \gamma[\mathbf{S} \times \mathbf{H}]$. Bloch proposed the phenomenological dissipative equation:

$$\frac{d\mathbf{S}}{dt} = \gamma[\mathbf{S} \times \mathbf{H}] - \frac{S_x}{T_2}\hat{x} - \frac{S_y}{T_2}\hat{y} + \frac{S_0 - S_z}{T_1}\hat{z}, \quad (1)$$

where S_0 is the thermal equilibrium spin and T_1 and T_2 are the longitudinal and transverse relaxation times [13]. The transverse relaxation is due to spin–spin interactions, while the longitudinal relaxation comes about because Zeeman energy is transferred to other degrees of freedom. We apply a rotational magnetic field $\mathbf{H}_{rot} = H_1 \cos(\omega_L t)\hat{x} + H_1 \sin(\omega_L t)\hat{y}$ during the pulse duration $t_{\pi/2} = \pi/(4\gamma H_1)$ to the spin initially polarized in the z direction. Supposing $t_{\pi/2} \ll T_1, T_2$ as usual, the spin tilts with Larmor precession to the $-y$ direction, being little affected by the relaxations. The relaxation of spin after the pulsed rotational field is turned off is described by the solution

$$\mathbf{S} = S_0\{\sin\omega_L t e^{-t/T_2}\hat{x} - \cos\omega_L t e^{-t/T_2}\hat{y} + (1 - e^{-t/T_1})\hat{z}\}. \quad (2)$$

Inhomogeneity of magnetic fields makes the Larmor frequency for each spin spatially dependent, causing dephasing of the spins during precession and decaying of the transverse signal. Spin echo, however, can recover the signal. This mechanism is different from that of the spin–spin relaxation characterized by T_2 . The spin echo of the combination of the $\pi/2$ – π pulse is effective. After a $\pi/2$ pulse, the angle ϕ between the spin $\mathbf{S}(\mathbf{r})$ and the x -axis is $-\pi/2$. The spin precesses with frequency $\omega(\mathbf{r}) = \gamma H_z(\mathbf{r})$ in the inhomogeneous field $H_z(\mathbf{r})\hat{z}$. If the distribution of the frequency is Gaussian $f(H_z - H_0) = 1/(\sqrt{2\pi}\sigma)\exp[-\gamma^2(H_z - H_0)^2/2\sigma^2]$, the time development of the y component of \mathbf{S} with T_2 relaxation becomes

$$\begin{aligned} S_y(t) &= S_0 \int_{-\infty}^{\infty} d\gamma H_z f(H_z - H_0) \sin\left(\gamma H_z t - \frac{\pi}{2}\right) e^{-\frac{t}{T_2}} \\ &= -S_0 \cos(\gamma H_0 t) \exp\left[-\frac{\sigma^2 t^2}{2} - \frac{t}{T_2}\right]. \end{aligned} \quad (3)$$

Immediately applying a π pulse at $t = \tau$, the spin reverses direction and the angle ϕ becomes $5/2\pi - \omega\tau$. Then S_y

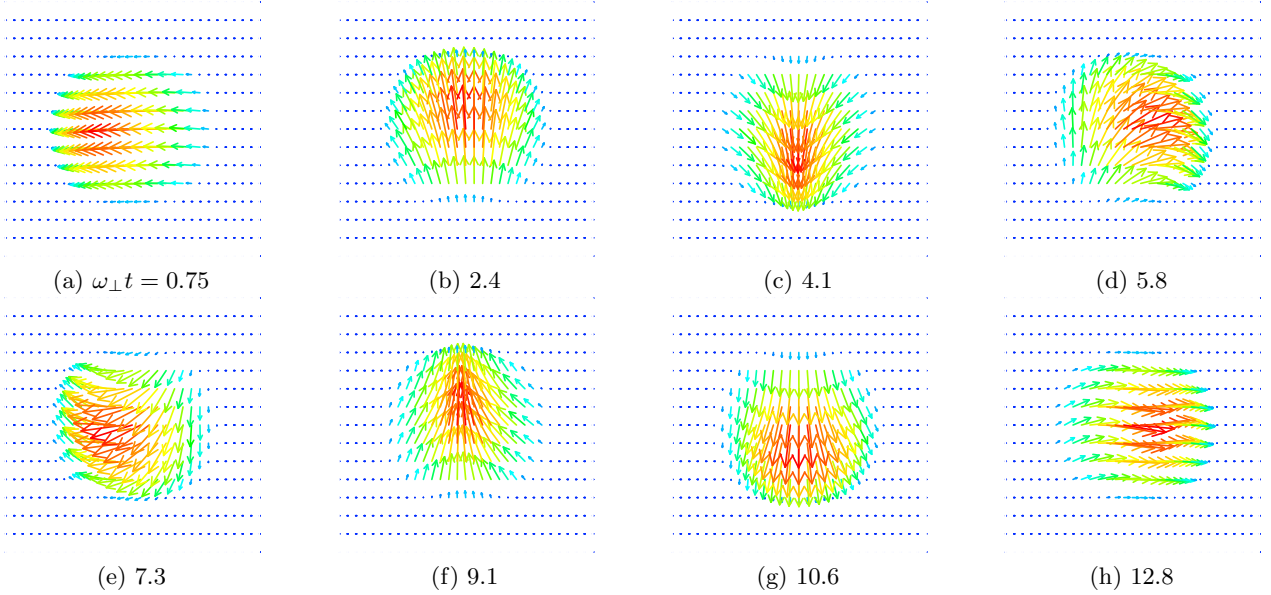


FIG. 1: (color online) Time development of the spin density vectors \mathbf{S} projected on the x - y plane in the spin echo with $\omega_{\perp}\tau = 5$. The magnitude of \mathbf{S} increases from blue to red.

develops as $S_y = S_0 \cos\{\gamma H_z(t' - \tau)\}$ with the new time variable t' after the pulse and the Gaussian distribution of H_z gives

$$S_y(t') = S_0 \cos\{\gamma H_0(t' - \tau)\} \times \exp\left[-\frac{\sigma^2(t' - \tau)^2}{2} - \frac{t' + \tau}{T_2}\right]. \quad (4)$$

Therefore, the signal recovers at $t' = \tau$, which is called spin echo. However, Eq. (4) shows that the peak of the echo cannot recover perfectly because of T_2 ; the spin echo can recover only the coherence lost by the inhomogeneity of the magnetic field, not the coherence lost by the spin-spin interaction.

To obtain spin echo in a ^{87}Rb BEC trapped by a harmonic potential of frequency ω_{\perp} , we study the two-dimensional spin-1 Gross-Pitaevskii (GP) equations with the MDDI:

$$i\hbar \frac{\partial \psi_{\alpha}}{\partial t} = \left(-\frac{\hbar^2}{2M} \nabla^2 + V_{trap} - \mu\right) \psi_{\alpha} - g\mu_B H_i S_{\alpha\beta}^i \psi_{\beta} + c_0 \psi_{\beta}^* \psi_{\beta} \psi_{\alpha} + c_2 S_i S_{\alpha\beta}^i \psi_{\beta} + c_{dd} \int d\mathbf{r}' \frac{\delta_{ij} - 3e^i e^j}{|\mathbf{r} - \mathbf{r}'|^3} S_i(\mathbf{r}') S_{\alpha\beta}^j \psi_{\beta}. \quad (5)$$

Here $V_{trap} = M\omega_{\perp}^2(x^2 + y^2)/2$ is the trapping potential, μ the chemical potential, g the Landé's g-factor, μ_B the Bohr magneton, and

$$S_i = \sum_{\alpha, \beta} \psi_{\alpha}^* S_{\alpha\beta}^i \psi_{\beta} \quad (6)$$

is the component of the spin density vector \mathbf{S} represented by the spin matrices $S_{\alpha\beta}^i$. The short range interaction constants are $c_0 = 4\pi\hbar^2(a_0 + 2a_2)/3M$ and

$c_2 = 4\pi\hbar^2(a_2 - a_0)/3M$ given by the s-wave scattering lengths a_0 and a_2 . The long range interaction constant is $c_{dd} = \mu_0 g^2 \mu_B^2 / 4\pi$ with vacuum magnetic permeability μ_0 . For ^{87}Rb , the parameters satisfy the relation $c_{dd} < -c_2 \ll c_0$ [7]. We investigate the spin echo under a gradient magnetic field $\mathbf{H} = (Gx + H_0)\hat{z}$ with constant G .

The dynamics start from the stationary states with $|c_{dd}/c_2| = 0$ and 0.02 in a gradient magnetic field of magnitude $0.98H_0 < |\mathbf{H}| < 1.02H_0$. Applying a \mathbf{H}_{rot} with $H_1 = 0.1H_0$, we calculate the GP equation using the Crank-Nicolson method, obtaining the spin echoes and effects of dephasing in the echo.

Spin echo is clearly observed in Fig. 1, showing the dynamics of \mathbf{S} projected on a x - y plane for $c_{dd} = 0$ and $\omega_{\perp}\tau = 5$. After the $\pi/2$ pulse, the spins are oriented in the $-y$ axis (Fig. 1(a)) and start precessing on the plane. Then, the precessions gradually diffuse because the Larmor frequency is spatially dependent due to the gradient magnetic field (Fig. 1(b), (c)). At $t = \tau + t_{\pi/2}$ (Fig. 1(d)), the π pulse is applied, which reverses the direction of the spin (Fig. 1(e)). The spins then gradually become coherent (Fig. 1(f), (g)), eventually refocusing at $t_{peak} = 2\tau + t_{\pi/2} + t_{\pi}$ (Fig. 1(h)). After the echo, the spins start to defocus again. These features are represented in the time development of the expectation value $\langle \hat{S}_{y,z} \rangle = \int d\mathbf{r} \psi_{\alpha}^* S_{\alpha\beta}^{y,z} \psi_{\beta}$ in Fig. 2. The signal of $\langle \hat{S}_y \rangle$ gradually decays from $t_{\pi/2}$ (a) to $\tau + t_{\pi/2}$ (d) and then increases from $\tau + t_{\pi/2} + t_{\pi}$ (e) to $2\tau + 3t_{\pi/2}$ (h).

To show that this is genuine spin echo, we investigate t_{peak} by changing τ , thus confirming the spin echo for $|c_{dd}/c_2| = 0$ and 0.02. Figure 3 indicates that the relation is satisfied until $\omega_{\perp}\tau = 6.5$ for $c_{dd} = 0$ and 4.5

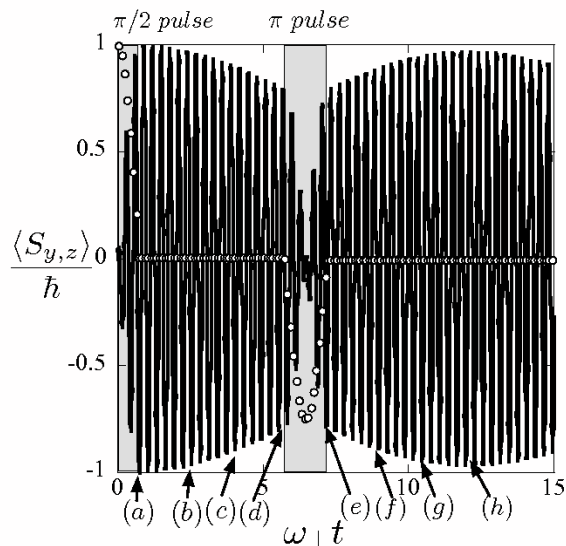


FIG. 2: Time development of $\langle S_y \rangle / \hbar$ (black line) and $\langle S_z \rangle / \hbar$ (white circles). The symbols (a)–(h) indicate the times shown in Fig. 1. The gray zones represent the intervals of the pulses. The behavior of $\langle \hat{S}_z \rangle / \hbar$ shows that the T_1 relaxation is irrelevant to the dynamics $\langle \hat{S}_y \rangle / \hbar$.

for $|c_{dd}/c_2| = 0.02$. These deviations from the relation $t_{peak} = 2\tau + 3t_{\pi/2}$ can be understood by investigating the equation of motion of spin based on the GP equations. From Eqs. (5) and (6), we obtain the equation of motion

$$\frac{\partial S_i}{\partial t} = \frac{1}{M} \nabla \cdot (S_{\beta\alpha}^i \mathbf{J}_{\alpha\beta}) + \gamma [\mathbf{S} \times \mathbf{H}]_i + \frac{c_{dd}}{\hbar} R_{dd}^j S_{l \neq \{i,j\}}, \quad (7)$$

where $\mathbf{J}_{\alpha\beta} = \hbar/2i(\psi_{\beta}^* \nabla \psi_{\alpha} - \psi_{\alpha} \nabla \psi_{\beta}^*)$ is the current of the momentum density and $R_{dd}^j = \int d\mathbf{r}' \frac{\delta_{jk} - 3e^j e^k}{|\mathbf{r} - \mathbf{r}'|^3} S_k(\mathbf{r}')$. The first, second, and third terms of Eq. (7) are derived from the kinetic, Zeeman, and MDDI terms of the GP equation. The differences between the circles and triangles in Fig. 3 are due to the dipole term, while their deviations from $t_{peak} = 2\tau + 3t_{\pi/2}$ are caused by the separation of the condensates due to the gradient magnetic field.

The magnetic resonance of this system is greatly affected by separation of spinor condensates. As shown in Fig. 4 (a), (b), (c), the condensates separate under the gradient field after the $\pi/2$ pulse, keeping approximate symmetry between $x > 0$ and $x < 0$. Applying the π pulse changes the ψ_1 and ψ_{-1} components to ψ_{-1} and ψ_1 respectively, which reverses \mathbf{S} . The π pulse breaks the symmetry of the distribution of the condensates. After the pulse, $\psi_{\pm 1}$ move to the center, tending to overlap each other for $\omega_{\perp} \tau < 7.5$. The overlap is not clear for $\omega_{\perp} \tau > 7.5$. The effect is caused by a repulsive interaction between the different components, which is easily found in the GP equations of Eq. (5). Thus, spin echo works properly for pulses shorter than $\omega_{\perp} \tau = 7.5$,

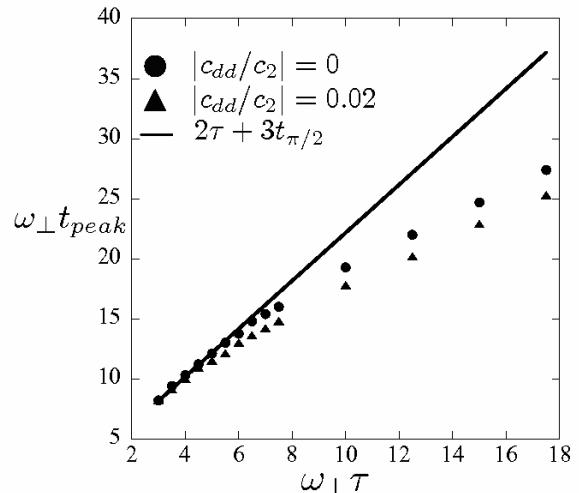


FIG. 3: Time $\omega_{\perp} t_{peak}$ at which echoes appear versus the interval $\omega_{\perp} \tau$ between $\pi/2$ and π pulses. The circles and triangles are the results for $|c_{dd}/c_2| = 0$ and 0.02 , respectively.

because phase separation is not yet significant. On the other hand, the MDDI operates as an attraction between ψ_1 and ψ_{-1} and makes the echo peaks appear earlier than the echo without the MDDI, as shown in Fig. 3.

We now apply Methods A and B, which are major sequences in NMR and ESR for measuring two relaxation times, to spinor condensates. The dynamics of Eq. (7) is characterized by two relaxation times. One is the relaxation time T_{nu} due to the non-uniform condensates and the other is the dipolar relaxation time T_{dd} . In Method A, the decay of echo peaks is measured using a $\pi/2$ – π pulse sequence for various values of τ . In liquids and gasses, the decay is generally caused by atomic self-diffusion; the first term of Eq. (7) operates similarly in our systems. In Method B, a $\pi/2$ – π – π ... pulse sequence is used, with n times π pulses applied after a $\pi/2$ pulse. Carr *et al.* introduced the effect of diffusion on liquids and gasses into the decay of a signal by using a random walk model and obtained transversal decay of the $\pi/2$ – π sequence $\exp[-t/T_2 - \gamma^2 a^2 G^2 t^3 / 24 n^2 \tau][2]$, where a is a fixed distance of the random walk. Thus, the diffusion decreases with increasing n . The diffusion is given by the first term of Eq. (7) in our case. For investigating T_{nu} and T_{dd} , we performed a numerical simulation of Methods A and B, shown in Fig. 5. Figure 5 (a) shows multiple exposures of $\langle \hat{S}_y \rangle / \hbar$ at $t = t_{peak}$ for various τ for Method A. The echo peaks decay with τ . When the condensates separate for large τ , the decay does not satisfy the exponential behavior. Thus, we fit the exponential formula to the echo peaks until $\omega_{\perp} \tau = 7.5$, obtaining a diffusion time of $\omega_{\perp} t = 40$ when $\langle \hat{S}_y \rangle / \hbar$ decays to e^{-1} . This diffusion time should be equal to T_{nu} . Figure 5 (b) shows a single exposure of the echo peaks for

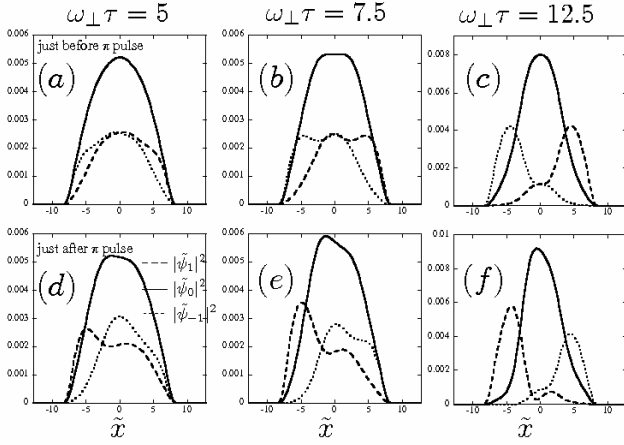


FIG. 4: Density profiles $|\tilde{\psi}_\alpha(y=0)|^2 = a_h^2 |\psi_\alpha(y=0)|^2 / N$ with $a_h = \sqrt{\hbar / M \omega_\perp}$ and $\tilde{x} = x / a_h$ without the MDDI just before the π pulse ((a), (b), (c)) and just after the π pulse ((d), (e), (f)) for $\omega_\perp \tau = 5, 7.5,$ and 12.5 .

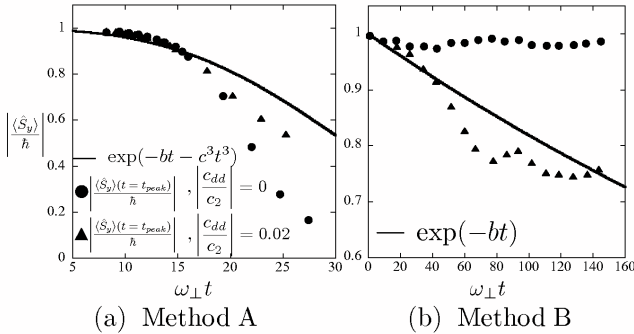


FIG. 5: (a) Results of Method A, showing multiple exposures of $\langle \hat{S}_y \rangle / \hbar$ with (circles) and without (triangles) the MDDI at t_{peak} for various τ , where $\omega_\perp \tau = 3.5, 4.0, \dots, 7.5, 10, 12.5, 15, 17.5$. The black line shows the Carr-Purcell form $\exp[-bt - c^3 t^3]$ with $b/c = 0.072$. (b) Results of Method B, showing a single exposure of the signal of peaks with $\omega_\perp \tau = 3.5$ and $n = 17$. The line $\exp(-bt)$ is fit to the early peaks, which are little affected by $\exp(-c^3 t^3 / 17^2)$. We obtain $\omega_\perp T_{dd} \sim 500$.

Method B with $\omega_\perp \tau = 3.5$ and $n = 17$. In the simulation, rather than applying the original $\pi/2 - \pi - \pi \dots$ sequence, we apply a $\pi/2 - \pi - (-\pi) - \pi - (-\pi) \dots$ sequence, considered by Meiboom and Gill [14], to cancel deviation due to repeated π pulses. In the case of no MDDI, the echo peaks do not decay, showing that the Method B sequence removes the effect of phase separation. While the signal with the MDDI decays, the relaxation time should be given by $\omega_\perp T_{dd} \sim 500$. These results show $T_{nu} < T_{dd}$. Method B enables us to reveal the MDDI through T_{dd} in

spinor dipolar BECs even if the MDDI is too weak to be easily detected.

In conclusion, we have numerically realized spin echo in a trapped ^{87}Rb BEC by calculating the spin-1 two-dimensional GP equation. We have investigated how the spin echoes are affected by the phase separation and the dipole-dipole interaction. The equation of motion of the spin density (Eq. (7)) derived from the GP equation shows two relaxation times T_{nu} and T_{dd} . In order to distinguish T_{dd} from T_{nu} by using spin echo, we introduce Methods A and B, obtaining the relation $T_{nu} > T_{dd}$. The study of spin echo of spinor BECs will help develop the field of magnetic resonance in cold atomic BECs system and may be applicable to MRI in these systems. Although this work is limited to the two-dimensional case, three-dimensional spinor BECs, especially with the MDDI, should show interesting features depending on geometry. A study of three-dimensional spinor BECs will be reported soon elsewhere.

M. Y. acknowledges the support of a research fellowship of the Japan Society for the Promotion of Science for Young Scientists (Grant No. 209928). M. T. acknowledges the support of a Grant-in Aid for Scientific Research from JSPS (Grant No. 18340109) and a Grant-in-Aid for Scientific Research on Priority Areas from MEXT (Grant No. 17071008).

- [1] E. L. Hahn, Phys. Rev. **80**, 580 (1950).
- [2] H. Y. Carr and E. M. Purcell, Phys. Rev. **94**, 630 (1954).
- [3] D. Vollhard and P. Wölfle, *The Superfluid Phases of Helium 3* (Taylor and Francis, London, 1990)
- [4] L. Santos and T. Pfau, Phys. Rev. Lett. **96**, 190404 (2006).
- [5] Y. Kawaguchi, H. Saito, and M. Ueda, Phys. Rev. Lett. **96**, 080405 (2006); *ibid.* **97**, 130404 (2006).
- [6] H. Mäkelä and K. -A. Suominen, Phys. Rev. A **75**, 033610 (2007).
- [7] S. Yi, L. You and H. Pu, Phys. Rev. Lett. **93**, 040403 (2004).
- [8] M. Takahashi, S. Ghosh, T. Mizushima, and K. Machida, Phys. Rev. Lett. **98**, 260403 (2007).
- [9] A. Griesmaier, J. Werner, S. Hensler, J. Stuhler, and T. Pfau, Phys. Rev. Lett. **94**, 160401 (2005).
- [10] J. Stuhler, A. Griesmaier, T. Koch, M. Fattori, T. Pfau, S. Giovanazzi, P. Pedri, and L. Santos, Phys. Rev. Lett. **95**, 150406 (2005).
- [11] T. Lahaye, T. Koch, B. Froöhlich, M. Fattori, J. Metz, A. Griesmaier, S. Giovanazzi, and T. Pfau, Nature **448**, 672 (2007).
- [12] Y. Kawaguchi, H. Saito, and M. Ueda, Phys. Rev. Lett. **98**, 110406 (2007).
- [13] F. Bloch, Phys. Rev. **70**, 460 (1946).
- [14] S. Meiboom and D. Gill, Rev. Sci. Instr. **69**, 688 (1954).